Drive circuit design for aerospace semiconductor laser based on SiC device

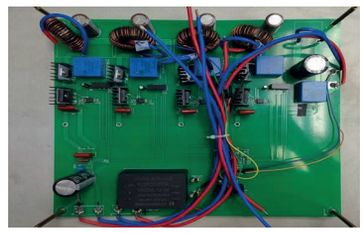

Diseño de circuito de accionamiento para un láser semiconductor aeroespacial basado en un dispositivo SiC

Xiaoqiang Zhang[1], Yunfeng Wang[1 *], Chunhui Wang[2] and Di Liu[3]

[1] North China University of Technology. Beijing Key Lab of Green Lighting Power Supply for Integration and Manufacture - Beijing 100144 (China).
[2] Shenhua Hollysys Information Technology Co., Ltd. Project Supervision Department (Safety Supervision Department) – 100011 Beijing (China).

DOI: https://doi.org/10.52152/D11386 | Recibido: 19/dec/2024 • Inicio Evaluación: 19/dec/2024 • Aceptado: 25/mar/2025

To cite this article: XIAOQIANG, Zhang; WANG, Yunfeng; WANG, Chunhui; LIU, Di. DRIVE CIRCUIT DESIGN FOR AEROSPACE SEMICONDUCTOR LASER BASED ON SiC DEVICE. DYNA July-August 2025, Vol. 100, n.4, pp. 321-327. DOI: https://dx.doi.org/10.6036/11386

FUNDING

This work was financially supported by Natural Science Foundation of Beijing, China (NO.3202009).

RESUMEN

- Los circuitos de accionamiento, que son la parte central de los láseres semiconductores, son cruciales para el campo de la ciencia y la tecnología aeroespacial, como la guía láser y la detección y medición de luz. Dada la altísima eficiencia cuántica de los láseres semiconductores, los cambios en la corriente afectan fácilmente a la estabilidad de la potencia de salida de los láseres semiconductores, lo que no favorece su uso seguro. Dado que la longitud de onda y la potencia de salida de los láseres semiconductores cambian considerablemente incluso con cambios menores en la corriente de excitación, en este estudio se analizaron las características de funcionamiento de los láseres semiconductores y se obtuvieron los requisitos de diseño del circuito de excitación de los láseres semiconductores aeroespaciales. Mediante la simulación de circuitos, se estableció un convertidor reductor paralelo intercalado de cuatro fases como topología principal del circuito de potencia del láser semiconductor, seguido de un análisis de modelado y un diseño de red de compensación para el convertidor mediante el método de promediado del espacio de estados. A continuación, el circuito de accionamiento se controló mediante el método de control de corriente media combinando el esquema de todo carburo de silicio, y el circuito de accionamiento prototipo se verificó experimentalmente. Los resultados demuestran que el circuito de accionamiento del láser semiconductor aeroespacial diseñado con un convertidor reductor paralelo intercalado de cuatro fases puede reducir el coeficiente de ondulación de la corriente de salida de 0,244 a 0,015, mejorar eficazmente la estabilidad del sistema de alimentación y mejorar notablemente la frecuencia de conmutación y la densidad de potencia del láser semiconductor. El algoritmo propuesto proporciona pruebas para la optimización y la evaluación del rendimiento de los controladores de láser semiconductor para aplicaciones aeroespaciales.
- **Palabras clave:** láser semiconductor, circuito de accionamiento, carburo de silicio, buck de cuatro fases, paralelo entrelazado.

ABSTRACT

Drive circuits, which are the core part of semiconductor lasers, are crucial to the field of aerospace science and technology, such as laser guidance and Light Detection and Ranging. Given the extremely high quantum efficiency of semiconductor lasers, changes in current easily affect the stability of the output power of semiconductor lasers, which is not conducive to their safe use. Given that the output wavelength and power of semiconductor lasers are considerably changed in the case of even minor changes in the drive current, the working characteristics of semiconductor lasers were analyzed in this study, and the drive circuit design requirements of aerospace semiconductor lasers were obtained. Through circuit simulation, a four-phase interleaved parallel buck converter was established as the main power circuit topology of the semiconductor laser, followed by modeling analysis and compensation network design for the converter through the state space averaging method. Then, the drive circuit was controlled through the average current control method combining the all-Silicon Carbide scheme, and the prototype drive circuit was experimentally verified. Results demonstrate that the drive circuit of the aerospace semiconductor laser designed with a four-phase interleaved parallel buck converter can reduce the ripple coefficient of the output current from 0.244 to 0.015, effectively improve the power system stability, and remarkably improve the switching frequency and power density of the semiconductor laser. The proposed algorithm provides evidence for the optimization and performance evaluation of semiconductor laser drivers for aerospace applications.

Keywords: Semiconductor laser, drive circuit, Silicon Carbide, four-phase buck, interleaving parallel..

1. INTRODUCTION

Semiconductor lasers work by injecting carriers, and through a certain excitation mode, the semiconductor substance transitions between energy bands to emit light and form a resonant cavity, realizing the particle number inversion of nonequilibrium carriers and exciting them to output a laser [3]. Given that a semiconductor laser is a junction device with extremely high quantum efficiency and high output power density, it cannot withstand electrical shock that is too strong. Meanwhile, the fluctuation of the drive current seriously affects the output stability of the laser,

which is not conducive to the safe use of the device. Excessive current fluctuation shortens the service life of the laser and even directly damages it [4].

In recent years, the design and optimisation of semiconductor laser driver circuits have received extensive attention, and scholars have made a series of breakthroughs in device characteristics and topology innovation.Du et al [5] systematically investigated the package parasitic effect of 6.5 kV SiC MOSFET/SBD by using a double-pulse test platform, and constructed an equivalent circuit model that revealed the influence of parasitic capacitance on the dynamic characteristics, but their study was not However, the study has not been extended to the integrated analysis of the circuit system composed of all SiC devices. In response to the miniaturisation requirements of laser drivers, Yang's team [6] innovatively proposed a solution based on GaN monolithic integration, which reduces the circuit size by 58% through three-dimensional packaging technology, however, the solution lacks the specific design and experimental validation of the driver circuit. In terms of energy efficiency optimization, Feng et al [7] proposed a dynamic regulation strategy for a four-phase interleaved buck topology based on the photovoltaic conversion efficiency curve, and experimentally showed that the efficiency was improved by 3.2 percentage points under 10A load, but the small-signal model of this topology was not established to support the closed-loop control design.Liu [8] conducted a study on the shunt characteristics of the LLC+Buck cascade topology, and revealed the impact of the duty cycle to turns ratio on the shunt accuracy, but this solution lacked specific design and experimental verification. Liu [8] studied the shunt characteristics of LLC+Buck cascade topology, revealing the influence of duty cycle and turns ratio on the shunt accuracy, but did not model and analyse the back-end interleaved Buck circuits. The two-phase interleaved topology designed by Sagar [9] for LV DC grids has a good equalisation of currents, but its efficiency characteristics and reliability in extreme aerospace environments (temperatures of -55~125°C and radiation doses >50krad) have not been verified. Current research presents two main technical features: one focuses on the characterisation of wide-bandwidth devices (e.g. Du's quantification of parasitic parameters in SiC packages, Yang's breakthrough in GaN integration), and the other focuses on architectural innovations in multiphase staggered topologies (e.g. Feng's four-phase buck strategy, Sagar's two-phase homogeneous current design). However, there are still significant limitations of the existing results for aerospace applications

In this study, a stable and reliable drive circuit for aerospace semiconductor lasers with a small ripple coefficient and high switching frequency was proposed. By analyzing the working characteristics of semiconductor lasers, the drive mode was determined. In accordance with the particularity of semiconductor lasers in aerospace, an all-SiC drive circuit was proposed, a four-phase interleaved parallel buck circuit model was established, and a compensation network was designed to implement the drive circuit for semiconductor lasers used in aerospace systems. Then, a prototype test of the four-phase interleaved parallel buck driver was performed to verify the correctness and feasibility of the method, and an efficiency test of the prototype was implemented to verify the effectiveness of the method. Results provided a basis for the optimization and performance evaluation of aerospace semiconductor lasers.

2. MATERIAL & METHODS

2.1. ANALYSIS OF FACTORS INFLUENCING THE OUTPUT POWER OF SEMICONDUCTOE LASERS

Semiconductor lasers are composed of countless laser diodes [10]. The I–V characteristic curve describes the relationship between the laser current and input voltage, and the P–I characteristic curve depicts the relationship between the laser-output optical power and input current [11]. As shown in Fig. 1(see section: supplementary material), I_{th} is the threshold current, and V_f stands for the break-over voltage.

In the drive circuit of a semiconductor laser, the minor fluctuation of the input voltage causes a great change in the output current, and the minor fluctuation of the current directly affects the output stability of the semiconductor laser. In the case of large drive current fluctuations, the laser may fail to work normally [12]. To guarantee the safe use and stable output of the semiconductor laser, the current-driven method [13] was adopted in this study.

Only when the output voltage of the drive circuit is higher than the threshold voltage of the semiconductor laser can the semiconductor laser inject current to work normally. However, the parameters of the semiconductor laser are closely related to the production process, and its internal parasitic parameters have almost no effect on the laser output, which can be ignored.

2.2. DRIVE CIRCUIT DESIGN METHOD FOR ACROSPACE SEMICONDUCTOR LASERS

2.2.1. Sic mosfet drive optimization method

In aerospace systems, the weight increases or decreases in grams; thus, small-sized, lightweight, and simply structured semiconductor lasers are often used. At the beginning of the 21st century, silicon carbide (SiC) technology has developed rapidly and its material properties are significantly better than those of conventional silicon (Si). As shown in Fig. 2 (see the Supplementary Materials section), SiC can withstand high voltages ranging from 600 V to thousands of volts by virtue of its wide bandwidth (up to 3.3 eV) and high dielectric breakdown field strength, while its stable crystal structure supports operating temperatures as high as 600 °C, which is much higher than the voltage and temperature limits of Si [14]. Thanks to the advantage of 2.3 times higher thermal conductivity than SiC devices can achieve high-frequency stable operation by combining twice the carrier saturation drift rate of Si while improving power density and integration. In addition, the low on-resistance characteristic significantly reduces system losses, resulting in a significant increase in the efficiency of SiC systems at the same power [15]. These performance advantages enable SiC devices to achieve high power output while significantly reducing size, component count and heat dissipation requirements, providing a key technology support for the balance between lightweight and high performance in aerospace.

To take full advantage of the extreme performance of silicon carbide, the all-SiC scheme was adopted, as shown in Fig. 3(see section: supplementary material). In consideration of the performance requirements of aerospace systems for device temperature, radiation resistance, and anti-interference, the SiC MOSFET and SiC SBD produced by Infineon, the world's leading SiC chip manufacturer, were selected to improve the power density of the system by reducing the energy consumption and cooling system.

The driver MOSFET chip adopts 1EDI20I12AH, which has independent source and sink outputs, and achieves the isolation barrier for data transmission through the indeterminate cavity transfor-

mer technology, and the isolation between the inputs and outputs greatly enhances the safety, and operates in a wide input voltage range; the separated rail-to-rail driver output simplifies the gate resistor selection, saves the external high-current bypass diode, and enhances the dv/dt control. Each driver features undervoltage lockout (UVLO) and active shutdown protection for logic inputs and drive outputs. Compared with similar chips, 1EDI20I12AH driver chip has the advantages of high reliability and easy design.

The final design of the driver circuit, as shown in Fig 4(see section: supplementary material) for a phase of the switching tube driver circuit. ISL6558 generated PWM signal through the 1EDI20I12AH electrical isolation and power amplification output to the switching tube, the driver resistor R1 and R2 were selected 3.3 Ω and 10 Ω, respectively, in order to meet the ability to drive fast. To meet the requirements of fast on and off, select the on voltage +18V, off voltage 0V, output drive current 4A.

2.2.2. Establishment of the four –phase interleaved parallel buck converter model

With the rapid development of aerospace technology, aerospace systems on the drive circuit puts forward more stringent requirements: in order to ensure that the volume of miniaturisation at the same time, but also need to meet the high current output, low ripple and high stability performance indicators. Although the traditional single-phase Buck circuit has the advantages of mature control technology, low cost, simple structure, etc., its inherent output current ripple, low power density and other defects, making it difficult to meet the special needs of the aerospace system. To solve this problem, the use of multi-phase interleaved parallel technology has become an ideal choice. The inductor current of each phase evenly shares the total output current, significantly reducing the single-phase current stress; secondly, the output filter capacitance can be reduced, which is conducive to the miniaturisation of the system; lastly, the total output current ripple can be much lower than the single-phase current ripple by the phase interleaving effect.

The choice of the number of phases N is crucial in the system design. As shown in Fig. 5 (see section: supplementary material), the output inductor current ripple as a function of duty cycle for a conventional single-phase, two-phase interleaved, three-phase interleaved, and four-phase interleaved shunt Buck converter under interleaved drive is compared. It can be seen that the maximum current ripple peak value of the converter output decreases with the increase of the number of parallel phases under the same switching frequency condition. The selection point to achieve zero current ripple duty cycle also increases with the increase of the number of parallel phases, which is extended to N-phase interleaved paralleling, the peak value of output current ripple will be lower or even close to zero.

By analysing the operating modes and output ripple laws of the multi-phase interleaved parallel Buck converter, it can be extended to the correspondence between the output current ripple of the N-phase interleaved parallel Buck converter and the system variables as shown in equation (1)

$$\Delta i_{LO}=\begin{cases}\dfrac{U_S}{L\cdot f}D & 0<\mathrm{DT}\le\dfrac{\mathrm{T}}{N}\\ \dfrac{U_S}{L\cdot f}(2-ND)\left(D-\dfrac{1}{N}\right) & \dfrac{\mathrm{T}}{N}<\mathrm{DT}\le\dfrac{2\mathrm{T}}{N}\\ \vdots & \vdots\\ \dfrac{U_S}{L\cdot f}\left((N-1)-ND\right)\left(D-\dfrac{N-2}{N}\right) & \dfrac{\mathrm{T}}{2}<\mathrm{DT}\le\dfrac{3\mathrm{T}}{4}\\ \dfrac{U_S}{L\cdot f}(N-ND)\left(D-\dfrac{N-1}{N}\right) & \dfrac{3\mathrm{T}}{4}<\mathrm{DT}\le T\end{cases} \quad (1)$$

The amplitude of the output current ripple at the corresponding duty cycle can be calculated from equation (1). In CCM mode, the output voltage ripple of the N-phase interleaved parallel converter is related to the duty cycle as shown in equation (2)

$$\Delta U_o=\frac{\Delta Q}{C}=\frac{U_S(1-D)D}{8\cdot C\cdot L\cdot(N\cdot f)^2} \quad (2)$$

According to Eq. 1, Eq. 2 and parametric indicators such as input voltage U_s, output voltage Uo and switching frequency, it is possible to determine the number of phases N of the converter in parallel, and the values of the capacity of inductors and capacitors of each phase Based on the analysis of system requirements, the four-phase structure shows significant advantages in topology selection: compared with the three-phase and below solutions, it can more effectively reduce the single-phase current stress and output ripple; compared with the more-phase solutions, the ripple

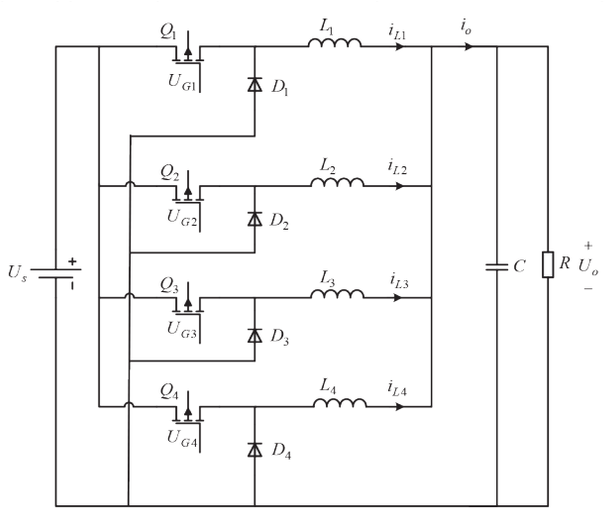

Fig. 6. Drive circuit topology of the semiconductor laser.

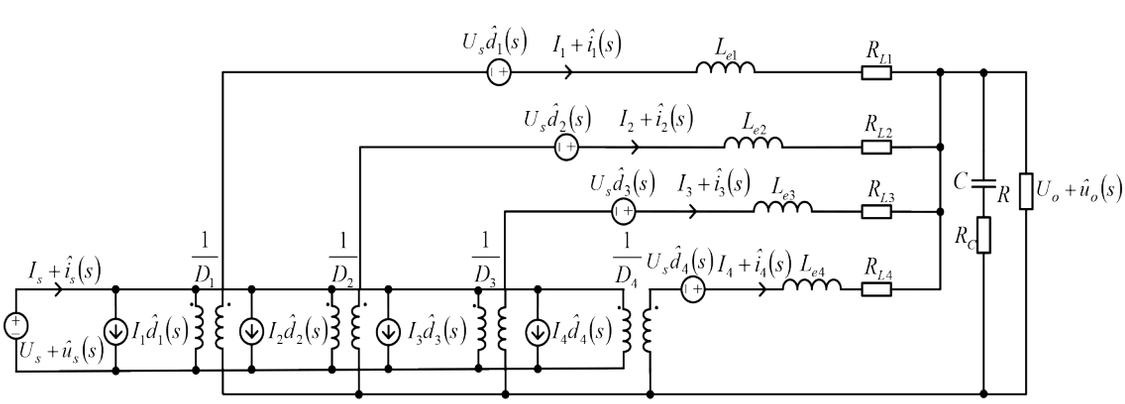

Fig. 7. AC small signal circuit model of a four-phase buck converter.

open-loop transfer function	four-phase	N-phase
$G_{u_o d_{k,(k=1,2,\cdots,N)}} = \frac{v_o}{d_k}$	$\frac{B}{A+4B}U_s$	$\frac{B}{A+NB}U_s$
$G_{i_k d_{k,(k=1,2,\cdots,N)}} = \frac{i_k}{d_k}$	$\frac{A+3B}{A^2+4AB}U_s$	$\frac{A+(N-1)B}{A^2+NAB}U_s$
$G_{i_k d_{m,m\neq k}^{(k=1,2,\cdots,N)}{}_{(k=1,2,\cdots,N)}} = \frac{i_k}{d_m}$	$-\frac{B}{A^2+4AB}U_s$	$-\frac{B}{A^2+NAB}U_s$
$G_{i_k i_{o,(k=1,2,\cdots,N)}} = \frac{i_k}{i_o}$	$\frac{B}{A+4B}$	$\frac{B}{A+NB}$
$Z_{out} = -\frac{u_o}{i_o}$	$-\frac{AB}{A+4B}$	$-\frac{AB}{A+NB}$

Table 1 Open-loop transfer function of multi-phase interleaved parallel Buck converter.

coefficient of the four-phase structure meets the design requirements under the premise of the four-phase structure to achieve the optimal balance between the complexity of the control and the size of the system. Fits the dual needs of high performance and miniaturisation of the aerospace system. Therefore, a four-phase interleaved shunt buck converter is finally adopted as the main circuit topology for the semiconductor laser.as shown in Fig. 6. L is the inductance, C stands for the filtering capacitance, U_s denotes the DC input voltage, and R represents the resistive load. Its principle is described as follows: four identical buck circuits are directly connected in parallel to ensure the amplitude consistency of each phase of the drive signal, and the conductive phase angle

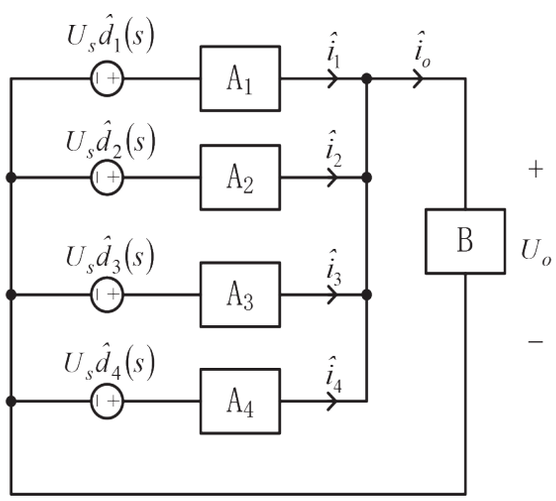

Fig. 8. Simplified equivalent circuit of the four-phase buck converter.

is successively spaced by 90°. While the total ripple is reduced, the working frequency is elevated to the four-fold frequency of the single-phase buck circuit.

The state space averaging method [16] was used to model the buck converter. In accordance with the modeling idea [17] of the ideal buck converter in the single-phase continuous conduction mode (CCM) mode and the equivalent circuit of the four-phase interleaved parallel buck converter, the alternating current (AC) small signal circuit model of the four-phase buck converter under the CCM mode was established, as shown in Fig. 7.

To obtain a simple AC small signal circuit model, Fig. 7. were simplified. Equation (3) was assumed as follows:

$$A_k = sL_k + R_{Lk}, k = 1,2,3,4$$

$$B = \left(\frac{1}{sC} + R_C\right) / /R = \frac{R(1+sCR_C)}{1+sC(R+R_C)} \quad (3)$$

where A_k is the state matrix, L_k denotes inductance, R_{LK} is the inductor resistance, B is the input matrix, C denotes capacitance, $R_C$is the capacitance resistance, and R denotes resistance.

Finally, the equivalent AC small signal circuit diagram was obtained, as shown in Fig. 8.

Under normal operation, the inductor current and capacitor voltage are state quantities. The input and state variables have 25 transfer functions, and all the parallel parameters are the same; that the module in Fig. 8 is the same. Analysis revealed that all transfer functions of the four-phase interleaved parallel buck converter can be obtained from five basic transfer functions: $G_{i_1 d1}$, $G_{i_2 d1}$, $G_{i_1 i_o}$, $G_{u_o d1}$, and Z_{out}.

When deriving the transfer function, only one input was assumed, and the other input was 0. With $d_1 \neq 0$, $d_{2,3,4} = 0$, and $i_o = 0$ set, $G_{u_o d1}$, $G_{i_1 d1}$, and $G_{i_2 d1}$ were obtained. $G_{i_1 i_o}$ and Z_{out} were solved by setting $d_{1,2,3,4} = 0$ and $i_o \neq 0$. The simplified four-phase interleaved shunt Buck converter AC small-signal model is solved for the open-loop transfer function and extended to the N-phase generic case, and the final derivation is summarised in Table 1.

Substituting Equation (3) into the Gvd(s) expression in Table 1 yields the control-output open-loop transfer function as:

$$\left.\frac{\hat{i}_o(s)}{\hat{d}(s)}\right|_{\hat{v}_s(s)=0} = \frac{V_s CRR_C s + RV_s}{(RLC + R_C LC)s^2 + (CRR_L + CR_L R_C + 4VRR_C + L)s + (4R + R_L)} \quad (4)$$

3. RESULTS

3.1. EXPERIMENTAL VERIFICATION OF THE COMPENSATION NETWORK

3.1.1. Verification example

To ensure the high switching frequency and low-output current ripple of the drive circuit, the related components and para-

meters of the main circuit were designed by taking a semiconductor laser driver in aerospace as an example.The main engineering parameters involved in this study are listed in Table 2(see section: supplementary material)

3.1.2. Compensation network

The Bode plot of the transfer function when no compensation network is added to the system is shown in Fig. 10(a), from which it is found that the system has a traversal frequency of 145 kHz and a phase margin of 90. which is less stable. A type III compensation network is introduced through research and analysis. The circuit is shown in Fig. 9(see section: supplementary material) and its transfer function is Equation. 3.

$$G_c(s)=\frac{K\left(1+\frac{s}{\omega_{z1}}\right)\left(1+\frac{s}{\omega_{z2}}\right)}{s\left(1+\frac{s}{\omega_{p1}}\right)\left(1+\frac{s}{\omega_{p2}}\right)},\ \omega_{z1}>\omega_{z2}>\omega_{p1}>\omega_{p2} \quad (5)$$

According to the engineering parameters and requirements, the crossover frequency of the system should be 15-25 kHz and the phase margin should be 45°-75°. To improve the stability of the system, the compensation network parameters of the four-phase interleaved shunt buck converter are calculated, and the K-factor method (Venable AN-103) and the Middlebrook stability criterion are used to complete the parameter design. R1 = 1 mΩ, R2 = 10 mΩ, R3 = 1 Ω, C1 = 44 nF, C2 = 4.7 μF, and C3 = 10 nF. MATLAB is used as the software platform to plot the Bode diagrams based on the transfer functions, and the Bode diagrams of the compensation network are shown in Fig. 10(b).

3.1.3. Result analysis

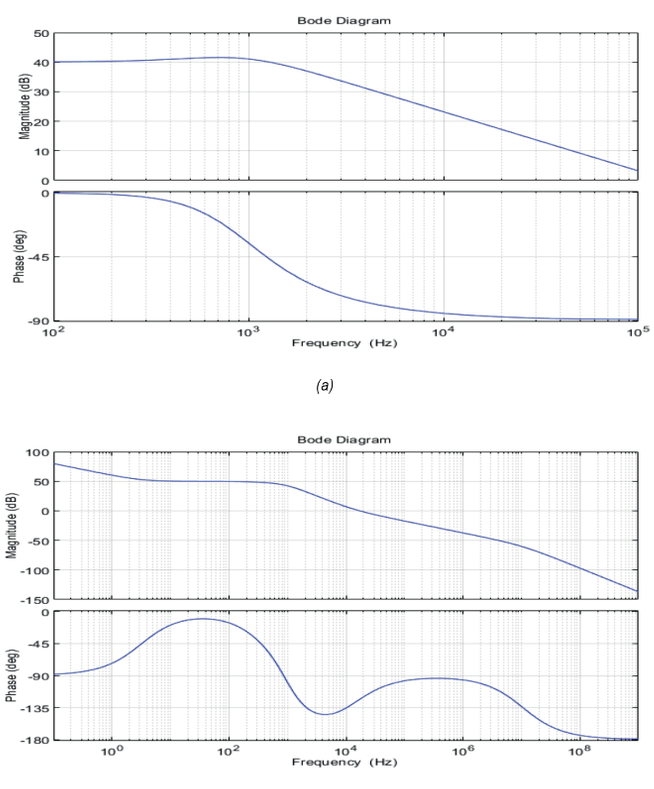

Fig. 10. Bode diagram of the transfer function. (a) without the compensation network; (b) with the compensation network.

After compensating the system, the crossover frequency was 17.1 kHz, and the phase margin was 56°, accompanied by a decline at the crossover frequency with a slope of –20 dB/dec, meeting the actual engineering requirements.

3.2. EXPERIMENTAL VERIFICATION OF THE FOUR-PHASE INTERLEAVED PARALLEL BUCK CONVERTER

3.2.1. Simulation experiment

Based on the Psim simulation platform, a conventional single-phase buck circuit and a four-phase interleaved shunt buck converter were simulated under the same conditions, and the topology of the four-phase interleaved shunt Buck circuit is shown in Fig. 11(see section: supplementary material). The input signals of the switching tubes, the output currents of the circuit and each output current of the four-phase interleaved shunt buck converter were measured.

3.2.2. Result analysis

The waveforms of the drive signal and output current of the traditional single-phase buck conversion circuit and four-phase interleaved parallel buck conversion circuit are shown in Fig. 12. The total output current of the single-phase buck conversion circuit was 20 A, and the ripple value was 2.5 A. The inductor current in each phase of the four-phase interleaved parallel buck conversion circuit was interleaved by 90° in turn, the output current was 20 A, and the ripple value was 0.2 A.

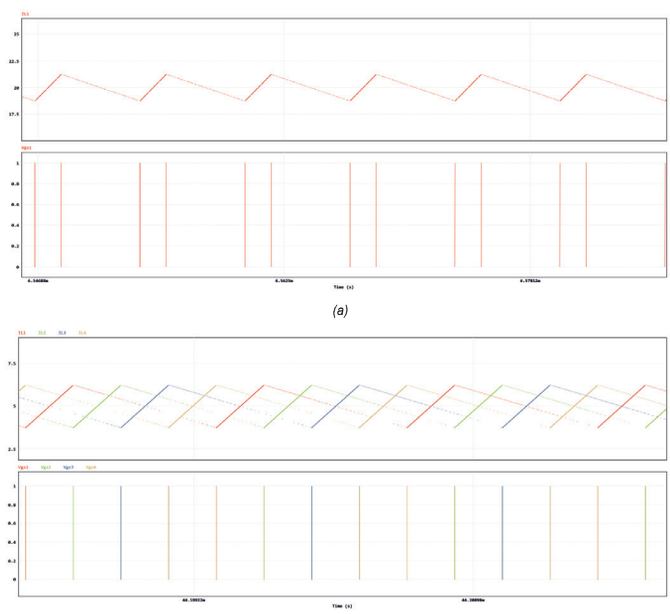

Fig. 12. Simulation experimental results. (a) Single-phase buck converter; (b) Four-phase interleaved parallel buck converter.

The comparison data of the simulation results are shown in Table 3(see section: supplementary material). Under the same input voltage, the four-phase interleaved parallel buck converter could effectively reduce the current of each phase of the inductor and the total output current ripple value in comparison with the traditional single-phase buck converter.

The analysis results revealed that the four-phase interleaved parallel buck converter could reduce the on–off loss of circuit power devices, improve the overall efficiency, and disperse the heat generated by each switching element, thus achieving the effect of improving the overall heat dissipation. Moreover, the fil-

tering volume and capacity of the circuit could be reduced while reducing the output ripple to a great extent.

3.3. TEST AND ANALYSIS OF THE DRIVE CIRCUIT FOR AEROSPACE SEMICONDUCTOR LASERS

3.3.1. Prototype test

In accordance with the technical indexes, an experimental prototype of a semiconductor laser driver was completed and experimentally verified, as shown in Fig. 13. The switching tube MOSFET and diode needed to withstand a voltage of 400 V, and the maximum current was $I_o = \Delta i_L / 2$. The overvoltage safety coefficient was not smaller than 1.5 times; thus, SiC MOSFET (model: IMW65R083M1H) and SiC (model: IDH20G65C6) diodes produced by Infineon were selected. In the inductor design, in order to prevent the occurrence of magnetic saturation phenomenon, it is necessary to select the appropriate size and material of the magnetic ring. In aerospace systems, the focus should consider the device's ability to resist radiation interference, so the design of the inductor should not only consider the impact of its magnetic field on the surrounding devices, but also consider the impact of radiation from other devices on the inductor, and ultimately, this paper selects the ring magnetic core. To reduce the energy loss on the inductor, and at the same time consider the price factor, this design adopts a highly reliable iron-silicon - aluminium powder ring, which has excellent magnetic properties, low power loss, high magnetic flux density, temperature resistance, humidity resistance and other characteristics. In consideration of a certain margin and the working mode, a CS400060 magnetic ring with an inductance of 200 μH and an electrolytic capacitor with a capacity of 600 and withstand voltage of 250 V were selected. The 1EDI20I12AH driver chip was packaged using PG-DSO-8-59 (top view). The ISL6558 controller with current sharing function is selected to achieve average current mode control based on the ISL6558 multi-phase PWM controller, and the control loop adopts a three-level cascade structure of voltage outer loop, current inner loop, and equal-current compensation loop, and is packaged in 16-SOIC.In the PCB layout [19], the SiC MOSFET drive circuit was connected with the switching tube through the Kelvin connection method to reduce the loss.

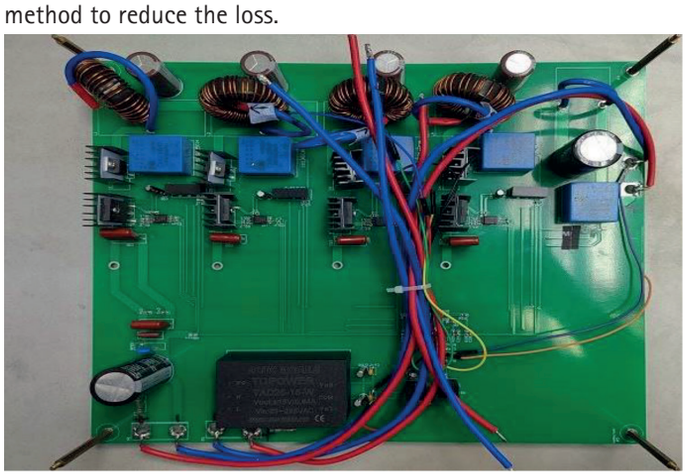

Fig. 13. Experimental prototype.

3.3.2. Test results

The output voltage of the system and the output voltage of the driver module were tested by using a voltage differential probe with strong anti-interference ability under an input voltage of 400 V and output no-load conditions. After the load was added, the inductor current of each phase and output current of the circuit were tested by a current probe, and the experimental waveforms are shown in Fig. 14.

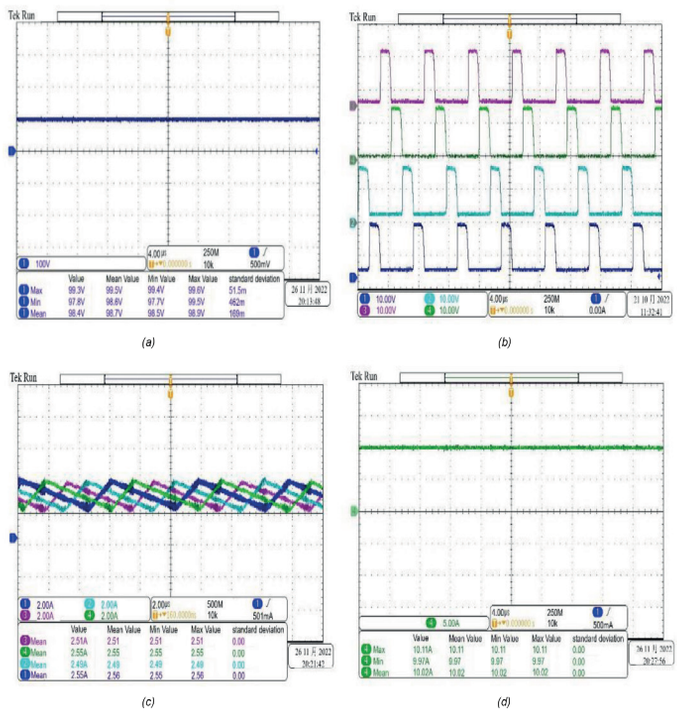

Fig. 14. Experimental waveforms. (a) Circuit output voltage; (b) Output of the driver module; (c) Inductor current of each phase; (d) Circuit output current.

The test results showed that the output voltage of the system was 98.4V, and the ripple coefficient was 0.015 when the input voltage was 400 V under output no-load conditions; moreover, the output energy could reach a stable state. After the control signal with an output amplitude of 3.6 V was amplified by the power of the driver module, the amplitude of the driver output signal was 16 V, the switching tube could be normally turned on, and the four-phase driving signal was turned on with a shift angle of 90°, which could stably drive the switching tube and realize the normal on/off operation of the four-way switching tube.

After loading, the four-phase currents were interleaved, the average current of the four-phase inductor current was 2.53 A, and the four-way current balance degree was 98.73%. Uniform current stress distribution, the system output was stable, and the balance effect was good. The output current of the system was 10.02 A, and the current ripple coefficient was 0.014. Compared with the single-phase output current, this circuit greatly reduced the ripple value of the output current and realized the functions of reducing the ripple, thereby increasing the frequency and stabilizing the output.

System efficiency is an important index to measure circuit performance. The efficiency of the designed circuit was tested, and the system efficiency at the output current moment of different loads is shown in Fig. 15(see section: supplementary material). The load current ranged from 1 A to 10 A, and the overall system efficiency was not lower than 95.4%. The circuit achieved a power output of 1 kW, which met the expected requirements.

The driver circuit is not only to meet the static characteristics of the stable measurement, but also has a fast dynamic response. In this paper, the dynamic characteristics of the output are measured by changing the output load using different relay switches, as shown in Figure 16(see section: supplementary material). In the moment of sudden change of load, the output voltage will produ-

ce a small change, and after about 50ms to reach a stable state, which can meet the expected results.

4. CONCLUSIONS

To study the effects of the drive circuit on the performance of the laser output and the service life of the laser and effectively reduce the ripple coefficient of the drive current, a drive circuit was designed for aerospace semiconductor lasers, and the all-SiC scheme was combined with a four-phase interleaved parallel buck converter. Then, modeling analysis and design of the four-phase interleaved parallel buck converter were conducted, the single-phase and four-phase interleaved parallel buck converters were compared through simulation, and the actual drive circuit prototype was experimentally verified. The following conclusions can be drawn:

(1) Based on the analysis of the structural features and characteristics of SiC materials, the use of all-silicon carbide devices has higher anti-irradiation performance compared with Si material devices, and at the same time, high-frequency stable operation can be achieved in the case of increased power density.

(2) Under the same duty cycle, the ripple of the output current decreases with the increase of the number of interleaved parallel phases, and the relationship between the output current ripple and the corresponding number of phases is obtained.

(3) Compared with the single-phase buck circuit, the aerospace semiconductor laser driver circuit designed with a four-phase interleaved parallel buck converter can reduce the ripple coefficient of the output current from 0.244 to 0.015, which can reduce the current stress in each phase of the switching tubes, reduce switching losses, and achieve the functions of reducing ripple, increasing frequency, and stabilising output.This method can effectively ensure the safe use and service life of aerospace semiconductor lasers.

In this study, the all-SiC scheme and four-phase interleaved parallel buck converter were combined, and the drive circuit of the aerospace semiconductor laser could effectively improve the strong influence of high semiconductor laser quantum efficiency on semiconductor output light intensity, which substantially guides research on aerospace semiconductor lasers. In this study, the control method of an analog circuit was mainly adopted. This circuit can be implemented through digital controllers, such as digital signal processing or field programmable gate arrays, in a follow-up study to improve the system accuracy.

REFERENCES

[1] Bogatov AP, Drakin AE. "Diode optical amplifier with phase control of the output wave for high-power laser systems with coherent beam combining". Journal of Physics D: Applied Physics. Mar. 2020. vol. 53-6. p. ID 065109. DOI: https://doi.org/10.1088/1361-6463/ab57c6

[2] Peng JW, Yu HY, Liu JG, et al. "Principles, Measurements and Suppressions of Semiconductor Laser Noise—A Review". IEEE Journal of Quantum Electronics. Oct. 2021. vol. 57-5. p. 1-15. DOI: https://doi.org/10.1109/JQE.2021.3093885

[3] Díaz SR. "A generalized theoretical approach for solar cells fill factors by using Shockley diode model and Lambert W-function: A review comparing theory and experimental data". Physica B: Physics of Condensed Matter. Jan. 2022. vol. 624. p. 413427. DOI: https://doi.org/10.1016/j.physb.2021.413427

[4] Cheng Q, Deng HQ. "Design of semiconductor laser drive circuit and temperature control system". Electron Device. Oct. 2019. vol. 42-05. p. 1185-1189. DOI: https://doi.org/10.3969/j.issn.1005-9490.2019.05.021

[5] Du YJ, Tang XL, Wei XG, et al. "Dynamic performance of 6.5 kV SiC MOSFET body diodes and anti-parallel Schottky barrier diodes". Power Electron. Mar. 2023. vol. 23. p. 1028-1040. DOI: https://doi.org/10.1007/s43236-023-00607-1

[6] Yang SX, Zhao BQ, Wang LJ, Wang N. "Adjustable narrow pulse laser drive circuit using GaN HEMT". Infrared and Laser Engineering. Oct. 2022. vol. 51-10. p. ID 20220036. DOI: https://doi.org/10.3788/IRLA20220036

[7] Feng, S. Y., Jin, K., Hui, Q., et al, "An Optimal Driving Strategy for Maximum Electro-optical Conversion Efficiency of Laser Diode in Laser Power Transmission System". In: 2019 IEEE Energy Conversion Congress and Exposition, Baltimore, MD, USA: IEEE, 2019, pp. 3348-3352. DOI: https://doi.org/10.1109/ECCE.2019.8912873

[8] Liu X, Zheng XJ, Hou QH, et al. "Current-sharing characteristic of converter composed of LLC with series-parallel transformer and interleaved Buck". Journal of Zhejiang University (Engineering Science). Apr. 2018. vol. 52-4. p. 806-818. DOI: https://doi.org/10.3785/j.issn.1008-973X.2018.04.026

[9] Sagar A, Sugali H, Bhisade S. "Design and Analysis of Robust Interleaved Buck Converter with Minimal Ripple Current". In: 2020 International Conference for Emerging Technology, Belgaum, India:IEEE, 2020, pp. 1-5. DOI: https://doi.org/10.1109/INCET49848.2020.9154168

[10] Byrne DC, Engelstaedter JP, Guo WH, et al. "Discretely Tunable Semiconductor Lasers Suitable for Photonic Integration". IEEE Journal of Selected Topics in Quantum Electronics. May. 2009. vol. 15-3. p. 482-487. DOI: https://doi.org/10.1109/JSTQE.2009.2016981

[11] Rondoni L, Ariffin M, Varatharajoo R, et al. "Optical complexity in external cavity semiconductor laser". Optics Communications. Mar. 2017. vol. 387. p. 257-266. DOI: https://doi.org/10.1016/j.optcom.2016.11.011

[12] Johnson LA. "Laser diode burn-in and reliability testing". IEEE Communications Magazine. Feb. 2006. vol. 44-2. p. 4-7. DOI: https://doi.org/10.1109/MCOM.2006.1593543

[13] ReyesPortillo IA, ClaudioSanchéz A, MoralesSaldaña JA, et al. "Study of the effects of current imbalance in a multiphase Buck converter for electric vehicles". World Electric Vehicle Journal. May. 2022. vol. 13-5. p. ID 88. DOI: https://doi.org/10.3390/wevj13050088

[14] Rothmund D, Bortis D, Kolar JW. "Highly compact isolated gate driver with ultrafast overcurrent protection for 10 kV SiC MOSFETs". CPSS Transactions on Power Electronics and Applications. Dec. 2018. vol. 3-4. p. 278-291. DOI: https://doi.org/10.24295/CPSSTPEA.2018.00028

[15] Deshpande A, Luo F. "Practical Design Considerations for a Si IGBT + SiC MOSFET Hybrid Switch: Parasitic Interconnect Influences, Cost, and Current Ratio Optimization". IEEE Transactions on Power Electronics. Jan. 2019. vol. 34-1. p. 724-737. DOI: https://doi.org/10.1109/TPEL.2018.2827989

[16] Zhang WP, Chen YA, Zhang M. Modeling and control of switching converter. Zhang WP (prologue writer). 1ª edición. Beijing: Mechanical Industry Press, 2019. 311 p. ISBN: 7-5083-3648-8

[17] Zhang WP, Zhang XQ, Mao P. Technology of switching power. Zhang WP (prologue writer). 1ª edición. Beijing: Mechanical Industry Press, 2021. 233 p. ISBN: 978-7-111-68203-5

[18] Rana N, Sonar S, Banerjee S. "Performance Investigation of Closed-Loop Dual Phase Interleaved Buck-Boost Converter With Dragonfly Optimized Type-III Controller". IEEE Transactions on Circuits and Systems II: Express Briefs. Mar. 2022. vol. 69-3. p. 1472-1476. DOI: https://doi.org/10.1109/TCSII.2021.3131567

[19] Cairnie, M., DiMarino, C., "Optimization of Electric-Field Grading Plates in a PCB-Integrated Bus Bar for a High-Density 10 kV SiC MOSFET Power Module". In: 2021 IEEE Applied Power Electronics Conference and Exposition, Phoenix, AZ, USA: IEEE, 2021, pp. 1464-1471. DOI: https://doi.org/10.1109/APEC42165.2021.9487102

SUPPLEMENTARY MATERIAL

https://www.revistadyna.com/documentos/pdfs/_adic/11386-1_en.pdf